

Information-Thermodynamic Bound on Information Flow in Turbulent Cascade

Tomohiro Tanogami¹ and Ryo Araki^{2,3}

¹*Department of Physics, Kyoto University, Kyoto 606-8502, Japan*

²*Graduate School of Engineering Science, Osaka University,
1-3 Machikaneyama, Toyonaka, Osaka 560-8531, Japan*

³*Univ. Lyon, École Centrale de Lyon, CNRS, Univ. Claude Bernard Lyon 1,
INSA Lyon, LMFA, UMR5509, 69130, Écully, France*

(Dated: January 11, 2023)

We investigate the nature of information flow in turbulence from an information-thermodynamic viewpoint. For the shell model with thermal noise, we show that information of large-scale eddies is transferred to small scales along with the energy cascade. The information transfer rate is characterized by the large-eddy turnover time. Furthermore, we numerically show that the information-thermodynamic efficiency is extremely low compared to other typical information processing systems such as Maxwell's demon. This result implies that transferring information from large to small scales involves enormous thermodynamic costs, indicating the poor performance of turbulence as an information processing system.

Introduction.—Various phenomena observed in complicated systems such as the Earth system [1–3] and chemical reaction network [4] can be regarded as nonequilibrium cooperative phenomena that emerge from many-body interactions. To elucidate and control the dynamics behind such phenomena, it is pertinent to focus on information transfer between components constituting the system. Particularly in mesoscopic systems affected by thermal fluctuations, the nature of such information transfer can be described by information thermodynamics [5]. Information thermodynamics is essentially stochastic thermodynamics for subsystems [6, 7] and provides constraints that are consistent with thermodynamics on the exchange of information between subsystems. Recently, it has been applied to information processing at the cellular level in biological systems [8–12] and even to deterministic chemical reaction networks [13].

Turbulent cascade is also a nonequilibrium cooperative phenomenon that emerges from extremely complicated interactions. In fully developed three-dimensional fluid turbulence, kinetic energy is transferred conservatively from large to small scales [14]. This energy cascade phenomenon can be described intuitively as the successive generation of smaller vortices by the stretching of larger vortices. Along with the energy cascade, fluctuations of small-scale quantities (e.g., the energy dissipation rate) follow those of large-scale quantities (e.g., the energy injection rate) with a time delay that corresponds to the large-eddy turnover time [15–17]. Moreover, the energy cascade induces chaos synchronization of small-scale motions, where small-scale velocity field is slaved to the chaotic dynamics of large-scale velocity field [18–22]. These phenomena suggest that information flow manifests the intrinsic characteristics of turbulence dynamics.

These observations motivate us to explore the nature of the information transfer across scales associated with turbulent cascade. Revealing the details of the information transfer process in turbulence may not only provide

insights into the generation mechanism of turbulent fluctuations leading to intermittency, but also allow comparative studies with other information processing systems. While turbulence has been studied in various contexts from such an information-theoretic viewpoint over recent decades [23–34], no previous studies have theoretically shown that information flows across scales along with turbulent cascade.

Here, we aim to elucidate the nature of information flow in fully developed three-dimensional fluid turbulence. To this end, we employ information thermodynamics by explicitly accounting for the thermal fluctuations inherent in fluid. From the second law of information thermodynamics, we can obtain universal constraints on information flow. Furthermore, this approach enables us to investigate the effects of thermal fluctuations on information transfer, which can affect the turbulence dynamics significantly [35–41]. While our approach can be applied to various turbulence models, here we use the stochastic Sabra shell model, which is a simplified caricature of the fluctuating Navier–Stokes equation in wave number space [42, 43]. This model has recently been used to investigate the effects of thermal fluctuations on turbulence [37, 38].

In this Letter, we prove that information of turbulent fluctuations is transferred from large to small scales along with the energy cascade. Our main result, (12) and (13), can be regarded as one of the few exact and universal results in the field of turbulence research. We numerically illustrate our findings and show that the rate of information transfer is characterized by the large-eddy turnover time. Furthermore, our numerical simulations suggest that the corresponding information-thermodynamic efficiency is quite low compared to other typical information processing systems such as Maxwell's demon. This implies that transferring information from large to small scales involves enormous thermodynamic costs, indicating the poor performance of turbulence as an information

processing system.

Setup.—We consider the Sabra shell model with thermal noise [37, 38, 44]. Let $u_n(t) \in \mathbb{C}$ be the “velocity” at time t with the wave number $k_n = k_0 2^n$ ($n = 0, 1, \dots, N$). The time evolution of the complex shell variables $u := \{u_n\}$ is given by the following Langevin equation:

$$\dot{u}_n = B_n(u, u^*) - \nu k_n^2 u_n + \sqrt{\frac{2\nu k_n^2 k_B T}{\rho}} \xi_n + f_n \quad (1)$$

with the scale-local nonlinear interactions given by

$$B_n(u, u^*) := i \left(k_{n+1} u_{n+2} u_{n+1}^* - \frac{1}{2} k_n u_{n+1} u_{n-1}^* + \frac{1}{2} k_{n-1} u_{n-1} u_{n-2} \right), \quad (2)$$

where we set $u_{-1} = u_{-2} = u_{N+1} = u_{N+2} = 0$. Here, $\nu > 0$ represents the kinematic viscosity, $f_n \in \mathbb{C}$ denotes the external body force that acts only at large scales, i.e., $f_n = 0$ for $n > n_f$, and $\xi_n \in \mathbb{C}$ is the zero-mean white Gaussian noise that satisfies $\langle \xi_n(t) \xi_{n'}^*(t') \rangle = 2\delta_{nn'} \delta(t-t')$. The specific form of the thermal noise term satisfies the fluctuation-dissipation relation of the second kind, where T denotes the absolute temperature, k_B the Boltzmann constant, and ρ the mass “density”.

Basic properties.—The nonlinear term $B_n(u, u^*)$ satisfies the following relation:

$$\sum_{n=0}^N (B_n(u, u^*) u_n^* + B_n^*(u, u^*) u_n) = 0. \quad (3)$$

Hence, the energy balance equation reads

$$\frac{d}{dt} \sum_{n=0}^N \frac{1}{2} \langle |u_n|^2 \rangle = - \sum_{n=0}^N \nu k_n^2 \langle |u_n|^2 \rangle + \sum_{n=0}^N \frac{2\nu k_n^2 k_B T}{\rho} + \varepsilon, \quad (4)$$

where $\varepsilon := \sum_{n=0}^{n_f} \langle u_n f_n^* + u_n^* f_n \rangle / 2$ denotes the energy injection rate. In the steady state, the energy injection rate balances the dissipation rate as follows:

$$\varepsilon \simeq \sum_{n=0}^N \nu k_n^2 \langle |u_n|^2 \rangle_{\text{ss}}. \quad (5)$$

Here, we have ignored the energy injection due to the thermal noise by noting that the kinetic energy is much larger than the thermal energy over a wide range of scales in turbulence [37, 38].

Shell models are known to exhibit rich temporal and multiscale statistics that are similar to those observed in real turbulent flow [45]. Most importantly, the model exhibits energy cascade. To see this, we consider the

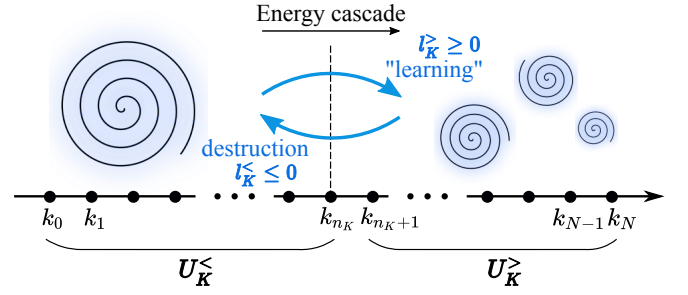


FIG. 1. (color online). Schematic of information flow in the energy cascade.

time evolution of the large-scale energy at the scales $k_n \leq K := k_{n_K}$ with $n_K \in \{n_f, \dots, N\}$,

$$\begin{aligned} \frac{d}{dt} \sum_{n=0}^{n_K} \frac{1}{2} \langle |u_n|^2 \rangle &= - \langle \Pi_K \rangle + \varepsilon \\ &\quad - \sum_{n=0}^{n_K} \nu k_n^2 \langle |u_n|^2 \rangle + \sum_{n=0}^{n_K} \frac{2\nu k_n^2 k_B T}{\rho}, \end{aligned} \quad (6)$$

where Π_K denotes the scale-to-scale energy flux from the large scales $k_n \leq K$ to the small scales $k_n > K$:

$$\Pi_K := - \frac{1}{2} \sum_{n=0}^{n_K} (B_n(u, u^*) u_n^* + B_n^*(u, u^*) u_n). \quad (7)$$

Because the viscous dissipation is negligible at scales much larger than the Kolmogorov dissipation scale $\eta \equiv k_\nu^{-1} := \nu^{3/4} \varepsilon^{-1/4}$, the last two terms on the right-hand side of (6) can be ignored within the inertial range $k_f \ll K \ll k_\nu$, where $k_f := k_{n_f}$. Hence, in the steady state, we obtain

$$\langle \Pi_K \rangle_{\text{ss}} = \varepsilon \quad \text{for } k_f \ll K \ll k_\nu. \quad (8)$$

The energy is thus transferred conservatively from large to small scales within the inertial range. Note that while the condition $k_f < K$ instead of $k_f \ll K$ is sufficient, we use the conventional definition for the inertial range.

Information-theoretic quantities.—Here, we introduce important quantities that characterize the information transfer among the shell variables. To quantify the information transfer across scales, we define the large-scale and small-scale shell variables as $\mathbf{U}_K^< := \{u_n, u_n^* | n \leq n_K\}$ and $\mathbf{U}_K^> := \{u, u^*\} \setminus \mathbf{U}_K^<$, respectively (see Fig. 1). The strength of the correlation between $\mathbf{U}_K^<$ and $\mathbf{U}_K^>$ is quantified by the mutual information (MI) [46]:

$$I[\mathbf{U}_K^< : \mathbf{U}_K^>] := \left\langle \ln \frac{p_t(\mathbf{U}_K^<, \mathbf{U}_K^>)}{p_t^<(\mathbf{U}_K^<) p_t^>(\mathbf{U}_K^>)} \right\rangle, \quad (9)$$

where $\langle \cdot \rangle$ denotes the average with respect to the joint probability distribution $p_t(\mathbf{U}_K^<, \mathbf{U}_K^>)$, and $p_t^<(\mathbf{U}_K^<)$ and

$p_t^>(\mathbf{U}_K^>)$ are the marginal distributions. The MI is non-negative and is equal to zero if and only if $\mathbf{U}_K^<$ and $\mathbf{U}_K^>$ are independent.

Because the MI is symmetric between the two variables, it cannot quantify the directional information flow from one variable to the other. The directional information flow can be quantified, e.g., using the *learning rate* (LR), which is also called the *information flow* [8, 11, 47, 48]. The LR that characterizes the rate at which $\mathbf{U}_K^<$ acquires information about $\mathbf{U}_K^>$ is defined as

$$l_K^< := \frac{I[\mathbf{U}_K^<(t+dt) : \mathbf{U}_K^>(t)] - I[\mathbf{U}_K^<(t) : \mathbf{U}_K^>(t)]}{dt}, \quad (10)$$

where the limit $dt \rightarrow 0^+$ is assumed. Similarly, the LR associated with $\mathbf{U}_K^>$ is defined by

$$l_K^> := \frac{I[\mathbf{U}_K^<(t) : \mathbf{U}_K^>(t+dt)] - I[\mathbf{U}_K^<(t) : \mathbf{U}_K^>(t)]}{dt}. \quad (11)$$

It follows from these definitions that $d_t I[\mathbf{U}_K^< : \mathbf{U}_K^>] = l_K^< + l_K^>$. Note that the LR can be either positive or negative. If $l_K^< > 0$ at time t , for example, then $\mathbf{U}_K^<$ acquires information about the instantaneous state $\mathbf{U}_K^>(t)$. In this sense, $\mathbf{U}_K^<$ is “learning” about or measuring $\mathbf{U}_K^>$. In contrast, if $l_K^< < 0$, then the correlation between $\mathbf{U}_K^<(t)$ and $\mathbf{U}_K^>(t)$ is destroyed or consumed. In particular, in the steady state, if $l_K^<$ is positive, then $l_K^>$ is negative because $l_K^< + l_K^> = 0$.

Main result.—In the steady state, for any K within the inertial range $k_f \ll K \ll k_\nu$, the LRs $l_K^<$ and $l_K^>$ satisfy the following inequalities:

$$0 \geq l_K^< \geq -\frac{\rho\varepsilon}{k_B T}, \quad (12)$$

$$\frac{\rho\varepsilon}{k_B T} \geq l_K^> \geq 0. \quad (13)$$

These inequalities are the main result of this Letter, which will be derived later. The inequality (12) implies that the large-scale shell variables $\mathbf{U}_K^<$ are destroying information about the small-scale variables $\mathbf{U}_K^>$ while transferring kinetic energy to small scales. In contrast, (13) states that the small-scale shell variables $\mathbf{U}_K^>$ are “learning” about $\mathbf{U}_K^<$ while receiving the kinetic energy from large scales (see Fig. 1). In particular, the maximum LR is given by $\rho\varepsilon/k_B T$.

Numerical simulation.—We here numerically illustrate the main result by estimating the LR. We set $N = 22$ and $n_f = 1$ to ensure that the external force acts only on 0th and 1st shells of the total 23 shells. The values of the external force and the other parameters are chosen following [37, 38] so that the achieved Reynolds number (Re) and the ratio of the thermal energy to the kinetic energy at the Kolmogorov dissipation scale are both comparable to the typical values in the atmospheric boundary layer, i.e., $\text{Re} \sim 10^6$ with $k_B T/\rho u_\eta^2 \sim 10^{-8}$, where $u_\eta := (\varepsilon\nu)^{1/4}$

denotes the characteristic velocity at the Kolmogorov dissipation scale. To investigate the Reynolds number dependence of the LR, we have also performed a simulation for a low Reynolds number, $\text{Re} \sim 10^5$, by setting $N = 19$. For both $N = 19$ and 22 cases, we have used $N_{\text{samp}} = 3 \times 10^5$ samples in the following averaging and estimation. Further details of the numerical simulation are given in [49].

Figure 2(a) shows the energy spectrum $E_n := \langle |u_n|^2 \rangle_{\text{ss}}/2$ in the steady state. The achieved Reynolds numbers are $\text{Re} \simeq 9.25 \times 10^4$ and 1.46×10^6 for the two cases $N = 19$ and 22, respectively. From this figure, we can see that the spectrum is consistent with the Kolmogorov spectrum in the inertial range, $E_n \propto k_n^{-2/3}$, while it exhibits the equipartition of energy in the dissipation range, $E_n = k_B T/\rho$.

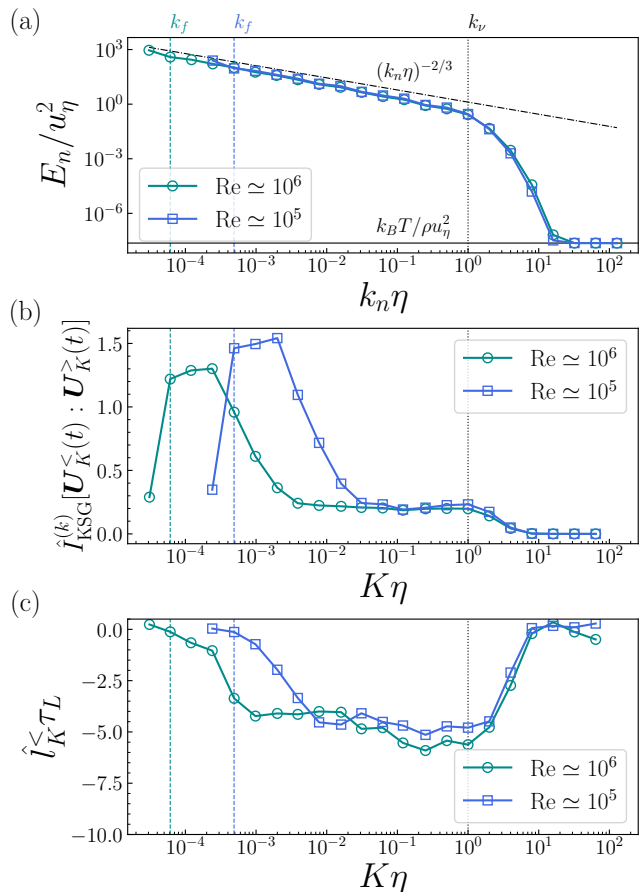


FIG. 2. (color online). (a) Scale dependence of the energy spectrum $E_n = \langle |u_n|^2 \rangle_{\text{ss}}/2$. The dash-dotted line represents $\varepsilon^{2/3} k_n^{-2/3}$. The solid line represents the thermal equipartition value $k_B T/\rho$. (b) Scale dependence of the estimated MI $\hat{J}_{\text{KSG}}^{(k)}[\mathbf{U}_K^<(t) : \mathbf{U}_K^>(t)]$ with $k = 4$. The error bars are within the marker size. (c) Scale dependence of the estimated LR $\hat{l}_K^<$. Note that it is plotted in units of the inverse of τ_L . In all panels, the dotted and dashed lines represent the Kolmogorov dissipation scale $k_\nu = 1/\eta$ and injection scale k_f , respectively.

We now estimate the LR defined by (10) and (11). To this end, we first estimate the MI. Note that the naive binning approach is not feasible in this case because it requires estimation of the $2(N+1)$ -dimensional probability density $p_t(\mathbf{U}_K^<, \mathbf{U}_K^>)$. Instead, we use the so-called Kraskov-Stögbauer-Grassberger (KSG) estimator [50–53], which has the advantage that it does not require estimation of the underlying probability density. The KSG estimator uses the distances to the k -th nearest neighbors of the sample points in the data to detect the structures of the underlying probability distribution. While we set $k = 4$ here, following [50], essentially the same result can be obtained for other values of k . Because the KSG estimator is based on the local uniformity assumption of the probability density, the estimated value approaches the true value as $N_{\text{samp}} \rightarrow \infty$ when this assumption is satisfied.

Figure 2(b) shows the estimated MI $\hat{I}_{\text{KSG}}^{(k)}[\mathbf{U}_K^<(t) : \mathbf{U}_K^>(t)]$. Its standard deviation is also estimated to be $\sim 10^{-3}$ by subsampling [52, 53], which lies within the marker size. Notably, the MI is almost independent of K in the inertial range, while it takes relatively large and small values in the injection and dissipation scales, respectively. This result reflects the dynamics that is scale-invariant in the inertial range while affected by external forces and thermal fluctuations in the injection and dissipation scales.

The LR can be estimated by substituting $\hat{I}_{\text{KSG}}^{(k)}$ into (10) or (11). Note that this procedure requires high accuracy in the estimation of the MI because the LR is defined through increments in the MI. Because it is not feasible to increase the number of samples, we instead take the approach of using the largest possible time increment Δt . Correspondingly, we focus only on $l_K^<$, because $l_K^>$ is defined through increments in the small-scale shell variables $\mathbf{U}_K^>$, which are fast variables relative to $\mathbf{U}_K^<$. We therefore estimate $l_K^<$, as defined by (10), using

$$\hat{l}_K^< := \frac{\hat{I}_{\text{KSG}}^{(k)}[\mathbf{U}_K^<(t + \Delta t) : \mathbf{U}_K^>(t)] - \hat{I}_{\text{KSG}}^{(k)}[\mathbf{U}_K^<(t) : \mathbf{U}_K^>(t)]}{\Delta t}. \quad (14)$$

Because we are interested in K within the inertial range, we choose Δt such that it is smaller than the smallest time scale in the inertial range. Therefore, we set $\Delta t = 0.1\tau_\eta$, where $\tau_\eta := \eta/u_\eta$ denotes the typical time scale at the Kolmogorov dissipation scale. Note that Δt is different from the time step $\delta t := 10^{-5}\tau_\eta$ used in solving (1) numerically.

In Fig. 2(c), we show the estimated LR $\hat{l}_K^<$ in units of the inverse of the large-eddy turnover time $\tau_L := 1/k_0 u_{\text{rms}}$, where $u_{\text{rms}}^2 := \sum_{n=0}^N \langle |u_n|^2 \rangle_{\text{ss}}$. For $\text{Re} \simeq 10^5$, we find that $\tau_L \simeq 181\tau_\eta$, while for $\text{Re} \simeq 10^6$, we find that $\tau_L \simeq 734\tau_\eta$. From this figure, we can see that the LR takes negative values for K within the inertial range. Because $(\rho\varepsilon/k_B T)\tau_L \simeq 7.79 \times 10^9$ for $\text{Re} \simeq 10^5$

and 3.15×10^{10} for $\text{Re} \simeq 10^6$, (12) is indeed satisfied. Interestingly, the lower bound of (12) is a loose bound. By noting that $l_K^< = -l_K^>$ in the steady state, this result states that the information-thermodynamic efficiency defined as $l_K^> k_B T / \rho\varepsilon$ is quite low [54]. In other words, the small-scale eddies acquire information about the large-scale eddies at a relatively high thermodynamic cost. This property is in contrast to other typical information processing systems such as Maxwell’s demon [11, 48, 54] and thus characterizes turbulence dynamics. Furthermore, Fig. 2(c) suggests that the LR can be scaled as $l_K^< \sim C/\tau_L$ in the inertial range, where C denotes a Re-independent dimensionless constant. By noting that τ_L can be interpreted as the characteristic time scale for the largest eddies to be stretched into smaller eddies, this result implies that the information of large-scale eddies is transferred to small scales by this stretching process.

Derivation of the main result.—The derivation of the main result is based on the second law of information thermodynamics for bipartite systems [54]. Specifically, we first formulate the second law of information thermodynamics for (1) by dividing the shell variables $\{u, u^*\}$ into the two groups $\mathbf{U}_K^<$ and $\mathbf{U}_K^>$, and then we take the inviscid limit $\nu \rightarrow 0$.

Let $S[\mathbf{U}_K^<]$ be the Shannon entropy of the large-scale shell variables, which is defined by $S[\mathbf{U}_K^<] := -\int d\mathbf{U}_K^< p_t^<(\mathbf{U}_K^<) \ln p_t^<(\mathbf{U}_K^<)$. The entropy increase in the heat bath associated with $\mathbf{U}_K^<$ is given by the sum of the contributions of each shell [55–57]:

$$\dot{S}_{\text{env}}^< = \sum_{n=0}^{n_K} \frac{\rho}{2k_B T} \langle u_n^* \circ (B_n(u, u^*) + f_n - \dot{u}_n) + \text{c.c.} \rangle, \quad (15)$$

where \circ denotes the multiplication in the sense of Stratonovich [58]. Similarly, let $S[\mathbf{U}_K^>]$ and $\dot{S}_{\text{env}}^>$ be the Shannon entropy and entropy increase in the heat bath associated with the small-scale shell variables $\mathbf{U}_K^>$, respectively. The second law of information thermodynamics is then given by [57]

$$\frac{d}{dt} S[\mathbf{U}_K^<] + \dot{S}_{\text{env}}^< \geq l_K^<, \quad (16)$$

$$\frac{d}{dt} S[\mathbf{U}_K^>] + \dot{S}_{\text{env}}^> \geq l_K^>. \quad (17)$$

If $\mathbf{U}_K^<$ and $\mathbf{U}_K^>$ are independent, then $l_K^< = l_K^> = 0$ and the standard second law of thermodynamics follows. In contrast, if they are correlated, then $l_K^<$ and $l_K^>$ can be either positive or negative.

We now assume that the system is in the steady state and set K to be within the inertial range $k_f \ll K \ll k_\nu$. Then, $\dot{S}_{\text{env}}^<$ and $\dot{S}_{\text{env}}^>$ can be expressed in terms of the

energy flux (7) as

$$\dot{S}_{\text{env}}^< = \frac{\rho}{k_{\text{B}}T} (\varepsilon - \langle \Pi_K \rangle_{\text{ss}}), \quad (18)$$

$$\dot{S}_{\text{env}}^> = \frac{\rho}{k_{\text{B}}T} \langle \Pi_K \rangle_{\text{ss}}, \quad (19)$$

where we have used $\Pi_{k_{\text{N}}} = 0$, which follows from (3). By substituting these expressions into (16) and (17) and by noting that $\langle \Pi_K \rangle_{\text{ss}} \rightarrow \varepsilon$ as $K/k_{\nu} \rightarrow 0$ and $l_K^< + l_K^> = 0$ in the steady state, we arrive at the main result (12) and (13).

Concluding remarks.—We have investigated the nature of information flow in turbulence from an information-thermodynamic viewpoint. Thermal fluctuations are crucial in deriving the universal relation (12) and (13) for information flow. On the other hand, it should be noted that the information flow itself is mainly governed by the large-scale dynamics rather than by the thermal fluctuations. In fact, the LR in the deterministic case ($T = 0$) is found to be almost the same as in the noisy case ($T > 0$) in the inertial range [59]. This result is consistent with the fact that the LR can be scaled as $l_K^< \sim C/\tau_L$ in the inertial range.

We now provide some technical remarks on estimation of the LR. Although the KSG estimator used here is asymptotically unbiased for $N_{\text{samp}} \rightarrow \infty$, there are a sample-size-dependent bias and a k -dependent bias for a finite N_{samp} in general [52, 53]. In our case, we have found that the magnitude of $\hat{I}_{\text{KSG}}^{(k)}[\mathbf{U}_K^< : \mathbf{U}_K^>]$ depends on k [53]. This may be because the probability distribution $p_t(\mathbf{U}_K^<, \mathbf{U}_K^>)$ is skewed and has heavy tails, thus violating the local uniformity condition [52]. Nevertheless, we have confirmed that the sign of $\hat{I}_K^<$ does not depend on the choice of k [53]. It should also be noted that the number of samples N_{samp} used here is not sufficient for high accurate estimation of the LR because the standard deviation of the estimated MI is comparable to its increment. In other words, if we naively estimate the error bar of the LR $\hat{I}_K^<$ by using the estimated standard deviation of the MI, it is of the same order as $\hat{I}_K^<$ itself. It is therefore desirable to perform the numerical calculations with higher accuracy while taking the bias into account.

Although we have focused on the Sabra shell model, similar results to those presented here would hold for other turbulence models, including the fluctuating Navier–Stokes equation [42, 43]. Because turbulent cascade is a ubiquitous phenomenon found in quantum fluids [60–63], supercritical fluids near a critical point [64], elastic bodies [65, 66], and even spin systems [67–69], it would be interesting to investigate the nature of the information flow in these various systems.

We thank Masanobu Inubushi, Wouter J. T. Bos, Susumu Goto, and Shin-ichi Sasa for fruitful discussions. We also thank Dmytro Bandak and Gregory L. Eyink for their helpful comments on the numerical simulation. T.T. is supported by JSPS KAKENHI Grant

No. 20J20079, a Grant-in-Aid for JSPS Fellows. R.A. is supported by the Takenaka Scholarship Foundation.

-
- [1] W. Steffen, J. Rockström, K. Richardson, T. M. Lenton, C. Folke, D. Liverman, C. P. Summerhayes, A. D. Barnosky, S. E. Cornell, M. Crucifix, *et al.*, Trajectories of the Earth System in the Anthropocene, *Proc. Natl. Acad. Sci. U. S. A.* **115**, 8252 (2018).
 - [2] M. Ghil and V. Lucarini, The physics of climate variability and climate change, *Rev. Mod. Phys.* **92**, 035002 (2020).
 - [3] J. Fan, J. Meng, J. Ludescher, X. Chen, Y. Ashkenazy, J. Kurths, S. Havlin, and H. J. Schellnhuber, Statistical physics approaches to the complex Earth system, *Phys. Rep.* **896**, 1 (2021).
 - [4] M. Feinberg, Foundations of chemical reaction network theory, (2019).
 - [5] J. M. Parrondo, J. M. Horowitz, and T. Sagawa, Thermodynamics of information, *Nat. Phys.* **11**, 131 (2015).
 - [6] U. Seifert, Stochastic thermodynamics, fluctuation theorems and molecular machines, *Rep. Prog. Phys.* **75**, 126001 (2012).
 - [7] L. Peliti and S. Pigolotti, *Stochastic Thermodynamics: An Introduction* (Princeton University Press, 2021).
 - [8] A. C. Barato, D. Hartich, and U. Seifert, Efficiency of cellular information processing, *New J. Phys.* **16**, 103024 (2014).
 - [9] P. Sartori, L. Granger, C. F. Lee, and J. M. Horowitz, Thermodynamic costs of information processing in sensory adaptation, *PLoS Comput. Biol.* **10**, e1003974 (2014).
 - [10] S. Ito and T. Sagawa, Maxwell’s demon in biochemical signal transduction with feedback loop, *Nat. Commun.* **6**, 1 (2015).
 - [11] D. Hartich, A. C. Barato, and U. Seifert, Sensory capacity: An information theoretical measure of the performance of a sensor, *Phys. Rev. E* **93**, 022116 (2016).
 - [12] S. Amano, M. Esposito, E. Kreidt, D. A. Leigh, E. Penocchio, and B. M. W. Roberts, Insights from an information thermodynamics analysis of a synthetic molecular motor, *Nat. Chem.* **14**, 530 (2022).
 - [13] E. Penocchio, F. Avanzini, and M. Esposito, Information Thermodynamics for Deterministic Chemical Reaction Networks, arXiv preprint arXiv:2204.02815 (2022).
 - [14] U. Frisch, *Turbulence* (Cambridge university press, 1995).
 - [15] T. Yasuda, S. Goto, and G. Kawahara, Quasi-cyclic evolution of turbulence driven by a steady force in a periodic cube, *Fluid Dyn. Res.* **46**, 061413 (2014).
 - [16] S. Goto, Y. Saito, and G. Kawahara, Hierarchy of antiparallel vortex tubes in spatially periodic turbulence at high Reynolds numbers, *Phys. Rev. Fluids* **2**, 064603 (2017).
 - [17] R. Araki, W. J. T. Bos, and S. Goto, Minimal modeling of the intrinsic cycle of turbulence driven by steady forcing, arXiv preprint arXiv:2112.03417 (2021).
 - [18] L. M. Pecora and T. L. Carroll, Synchronization in chaotic systems, *Phys. Rev. Lett.* **64**, 821 (1990).
 - [19] S. Boccaletti, J. Kurths, G. Osipov, D. Valladares, and C. Zhou, The synchronization of chaotic systems, *Phys. Rep.* **366**, 1 (2002).

- [20] K. Yoshida, J. Yamaguchi, and Y. Kaneda, Regeneration of small eddies by data assimilation in turbulence, *Phys. Rev. Lett.* **94**, 014501 (2005).
- [21] C. C. Lalescu, C. Meneveau, and G. L. Eyink, Synchronization of chaos in fully developed turbulence, *Phys. Rev. Lett.* **110**, 084102 (2013).
- [22] A. Vela-Martín, The synchronisation of intense vorticity in isotropic turbulence, *J. Fluid Mech.* **913** (2021).
- [23] R. Betchov, Measure of the intricacy of turbulence, *Phys. Fluids* **7**, 1160 (1964).
- [24] K. Ikeda and K. Matsumoto, Information theoretical characterization of turbulence, *Phys. Rev. Lett.* **62**, 2265 (1989).
- [25] R. T. Cerbus and W. I. Goldburg, Information content of turbulence, *Phys. Rev. E* **88**, 053012 (2013).
- [26] M. Materassi, G. Consolini, N. Smith, and R. De Marco, Information theory analysis of cascading process in a synthetic model of fluid turbulence, *Entropy* **16**, 1272 (2014).
- [27] R. T. Cerbus and W. I. Goldburg, Information theory demonstration of the Richardson cascade, arXiv preprint arXiv:1602.02980 (2016).
- [28] W. I. Goldburg and R. T. Cerbus, Turbulence as information, arXiv preprint arXiv:1609.00471 (2016).
- [29] C. Granero-Belinchon, S. G. Roux, and N. B. Garnier, Scaling of information in turbulence, *Europhys. Lett.* **115**, 58003 (2016).
- [30] C. Granero-Belinchón, S. G. Roux, and N. B. Garnier, Kullback-Leibler divergence measure of intermittency: Application to turbulence, *Phys. Rev. E* **97**, 013107 (2018).
- [31] A. Lozano-Durán, H. J. Bae, and M. P. Encinar, Causality of energy-containing eddies in wall turbulence, *J. Fluid Mech.* **882** (2020).
- [32] M. Shavit and G. Falkovich, Singular measures and information capacity of turbulent cascades, *Phys. Rev. Lett.* **125**, 104501 (2020).
- [33] N. Vladimirova, M. Shavit, and G. Falkovich, Fibonacci turbulence, *Phys. Rev. X* **11**, 021063 (2021).
- [34] A. Lozano-Durán and G. Arranz, Information-theoretic formulation of dynamical systems: Causality, modeling, and control, *Phys. Rev. Research* **4**, 023195 (2022).
- [35] D. Ruelle, Microscopic fluctuations and turbulence, *Phys. Lett. A* **72**, 81 (1979).
- [36] T. S. Komatsu, S. Matsumoto, T. Shimada, and N. Ito, A glimpse of fluid turbulence from the molecular scale, *Int. J. Mod. Phys. C* **25**, 1450034 (2014).
- [37] D. Bandak, G. L. Eyink, A. Mailybaev, and N. Goldenfeld, Thermal noise competes with turbulent fluctuations below millimeter scales, arXiv preprint arXiv:2107.03184 (2021).
- [38] D. Bandak, N. Goldenfeld, A. A. Mailybaev, and G. Eyink, Dissipation-range fluid turbulence and thermal noise, *Phys. Rev. E* **105**, 065113 (2022).
- [39] G. Eyink and A. Jafari, High schmidt-number turbulent advection and giant concentration fluctuations, *Phys. Rev. Research* **4**, 023246 (2022).
- [40] R. M. McMullen, M. C. Krygier, J. R. Torczynski, and M. A. Gallis, Navier-Stokes Equations Do Not Describe the Smallest Scales of Turbulence in Gases, *Phys. Rev. Lett.* **128**, 114501 (2022).
- [41] J. B. Bell, A. Nonaka, A. L. Garcia, and G. Eyink, Thermal fluctuations in the dissipation range of homogeneous isotropic turbulence, *J. Fluid Mech.* **939** (2022).
- [42] L. D. Landau and E. M. Lifshitz, *Fluid Mechanics*, Vol. 6 (Addison-Wesley, Reading, MA, 1959).
- [43] J. M. O. De Zarate and J. V. Sengers, *Hydrodynamic fluctuations in fluids and fluid mixtures* (Elsevier, 2006).
- [44] V. S. L'vov, E. Podivilov, A. Pomyalov, I. Procaccia, and D. Vandembroucq, Improved shell model of turbulence, *Phys. Rev. E* **58**, 1811 (1998).
- [45] L. Biferale, Shell models of energy cascade in turbulence, *Annu. Rev. Fluid Mech.* **35**, 441 (2003).
- [46] T. M. Cover and J. A. Thomas, *Elements of Information Theory*, 2nd ed. (Wiley-Interscience, Hoboken, NJ, 2006).
- [47] D. Hartich, A. C. Barato, and U. Seifert, Stochastic thermodynamics of bipartite systems: transfer entropy inequalities and a Maxwell's demon interpretation, *J. Stat. Mech.* **2014**, P02016 (2014).
- [48] T. Matsumoto and T. Sagawa, Role of sufficient statistics in stochastic thermodynamics and its implication to sensory adaptation, *Phys. Rev. E* **97**, 042103 (2018).
- [49] See Supplemental Material at [URL will be inserted by publisher] for the details of the numerical simulation.
- [50] A. Kraskov, H. Stögbauer, and P. Grassberger, Estimating mutual information, *Phys. Rev. E* **69**, 066138 (2004).
- [51] S. Khan, S. Bandyopadhyay, A. R. Ganguly, S. Saigal, D. J. Erickson III, V. Protopopescu, and G. Ostrouchov, Relative performance of mutual information estimation methods for quantifying the dependence among short and noisy data, *Phys. Rev. E* **76**, 026209 (2007).
- [52] C. M. Holmes and I. Nemenman, Estimation of mutual information for real-valued data with error bars and controlled bias, *Phys. Rev. E* **100**, 022404 (2019).
- [53] See Supplemental Material at [URL will be inserted by publisher] for the details of the KSG estimator and its variance and bias.
- [54] J. M. Horowitz and M. Esposito, Thermodynamics with continuous information flow, *Phys. Rev. X* **4**, 031015 (2014).
- [55] K. Sekimoto, *Stochastic Energetics* (Springer, New York, 2010).
- [56] J. M. Horowitz, Multipartite information flow for multiple Maxwell demons, *J. Stat. Mech.* , P03006 (2015).
- [57] See Supplemental Material at [URL will be inserted by publisher] for the derivation of the second law of information thermodynamics.
- [58] C. W. Gardiner, *Handbook of Stochastic Methods*, 4th ed. (Springer, Berlin, 2009).
- [59] See Supplemental Material at [URL will be inserted by publisher] for the deterministic case.
- [60] T. Tanogami, Theoretical analysis of quantum turbulence using the Onsager ideal turbulence theory, *Phys. Rev. E* **103**, 023106 (2021).
- [61] T. Tanogami, Reply to “Comment on ‘Theoretical analysis of quantum turbulence using the Onsager ideal turbulence theory’ ”, *Phys. Rev. E* **105**, 027102 (2022).
- [62] G. Krstulovic, V. L'vov, and S. Nazarenko, Comment on “Theoretical analysis of quantum turbulence using the Onsager ideal turbulence theory”, *Phys. Rev. E* **105**, 027101 (2022).
- [63] L. Skrbek, D. Schmoranzler, Š. Midlik, and K. R. Sreenivasan, Phenomenology of quantum turbulence in superfluid helium, *Proc. Natl. Acad. Sci. U. S. A.* **118** (2021).
- [64] T. Tanogami and S.-i. Sasa, Van der Waals cascade in supercritical turbulence near a critical point, *Phys. Rev. Research* **3**, L032027 (2021).
- [65] S. Nazarenko, *Wave Turbulence*, Vol. 825 (Springer Science & Business Media, 2011).

- [66] V. E. Zakharov, V. S. L'vov, and G. Falkovich, *Kolmogorov spectra of turbulence I: Wave turbulence* (Springer, Berlin, 1992).
- [67] T. Tanogami and S.-i. Sasa, XY model for cascade transfer, *Phys. Rev. Research* **4**, L022015 (2022).
- [68] M. Tsubota, Y. Aoki, and K. Fujimoto, Spin-glass-like behavior in the spin turbulence of spinor Bose-Einstein condensates, *Phys. Rev. A* **88**, 061601(R) (2013).
- [69] J. F. Rodriguez-Nieva, Turbulent relaxation after a quench in the Heisenberg model, *Phys. Rev. B* **104**, L060302 (2021).

Supplemental Material: Information-Thermodynamic Bound on Information Flow in Turbulent Cascade

Tomohiro Tanogami¹ and Ryo Araki^{2,3}

¹*Department of Physics, Kyoto University, Kyoto 606-8502, Japan*

²*Graduate School of Engineering Science, Osaka University,
1-3 Machikaneyama, Toyonaka, Osaka 560-8531, Japan*

³*Univ. Lyon, École Centrale de Lyon, CNRS, Univ. Claude Bernard Lyon 1,
INSA Lyon, LMFA, UMR5509, 69130, Écully, France*

S1. DERIVATION OF THE SECOND LAW OF INFORMATION THERMODYNAMICS

In this section, we explain the derivation of the second law of information thermodynamics for the stochastic Sabra shell model.

A. Formulation of the second law of thermodynamics

First, we formulate the standard second law of thermodynamics. Let $S[u, u^*] := - \int dud u^* p_t(u, u^*) \ln p_t(u, u^*)$ be the system entropy, where $dud u^* := \prod_n d\text{Re}[u_n] d\text{Im}[u_n]$, and $p_t(u, u^*)$ denotes the probability distribution function. Here, we use the notation $S[u, u^*]$ to indicate the relevant random variables (u, u^*) although $S[u, u^*]$ is not a function of (u, u^*) . The time evolution of $p_t(u, u^*)$ is governed by the following Fokker-Planck equation [1]:

$$\begin{aligned} \partial_t p_t(u, u^*) &= \sum_{n=0}^N \left[-\frac{\partial}{\partial u_n} (A_n(u, u^*) p_t(u, u^*)) - \frac{\partial}{\partial u_n^*} (A_n^*(u, u^*) p_t(u, u^*)) + \frac{4\nu k_n^2 k_B T}{\rho} \frac{\partial^2}{\partial u_n \partial u_n^*} p_t(u, u^*) \right] \\ &= \sum_{n=0}^N \left[-\frac{\partial}{\partial u_n} J_n(u, u^*) - \frac{\partial}{\partial u_n^*} J_n^*(u, u^*) \right], \end{aligned} \quad (\text{S1})$$

where

$$A_n(u, u^*) := B_n(u, u^*) - \nu k_n^2 u_n + f_n, \quad (\text{S2})$$

and $J_n(u, u^*)$ denotes the probability current,

$$J_n(u, u^*) := A_n(u, u^*) p_t(u, u^*) - \frac{2\nu k_n^2 k_B T}{\rho} \frac{\partial}{\partial u_n^*} p_t(u, u^*). \quad (\text{S3})$$

Therefore, the average rate of change of the system entropy is given by

$$\begin{aligned} \frac{d}{dt} S[u, u^*] &= -\frac{d}{dt} \int dud u^* p_t(u, u^*) \ln p_t(u, u^*) \\ &= - \int dud u^* (\partial_t p_t(u, u^*)) \ln p_t(u, u^*) - \int dud u^* p_t(u, u^*) \partial_t \ln p_t(u, u^*) \\ &= \int dud u^* \sum_{n=0}^N \left[\frac{\partial}{\partial u_n} J_n(u, u^*) + \frac{\partial}{\partial u_n^*} J_n^*(u, u^*) \right] \ln p_t(u, u^*) - \frac{d}{dt} \int dud u^* p_t(u, u^*) \\ &= \sum_{n=0}^N \dot{S}_n[u, u^*]. \end{aligned} \quad (\text{S4})$$

In the last line, we have introduced $\dot{S}_n[u, u^*]$, which is given by

$$\dot{S}_n[u, u^*] := - \int dud u^* \left[J_n(u, u^*) \frac{\partial}{\partial u_n} \ln p_t(u, u^*) + J_n^*(u, u^*) \frac{\partial}{\partial u_n^*} \ln p_t(u, u^*) \right], \quad (\text{S5})$$

where the over-dot denotes the rates of change of observables that are not a time derivative of a state function.

Let Δs^{env} be the stochastic medium entropy production in an infinitesimal time interval $[t, t + dt]$. To identify Δs^{env} , we impose the local detailed balance condition [2, 3]:

$$\Delta s^{\text{env}} = \ln \frac{p(u', u'^*, t + dt | u, u^*, t)}{p(-u, -u^*, t + dt | -u', -u'^*, t)}. \quad (\text{S6})$$

Here, the transition probability density $p(u', u'^*, t + dt | u, u^*, t)$ is given by, in the Ito scheme, [1]

$$p(u', u'^*, t + dt | u, u^*, t) = \prod_{n=0}^N \frac{\rho}{4\pi\nu k_n^2 k_B T dt} \exp\left(-\frac{\rho}{4\nu k_n^2 k_B T dt} |du_n - A_n(u, u^*)dt|^2\right), \quad (\text{S7})$$

where $du := u' - u$ with $u(t) = u$ and $u(t + dt) = u'$. Similarly, $p(-u, -u^*, t + dt | -u', -u'^*, t)$ is given by

$$p(-u, -u^*, t + dt | -u', -u'^*, t) = \prod_{n=0}^N \frac{\rho}{4\pi\nu k_n^2 k_B T dt} \exp\left(-\frac{\rho}{4\nu k_n^2 k_B T dt} |du_n - [-A_n^{\text{ir}}(u, u^*) + A_n^{\text{rev}}(u, u^*)] dt|^2\right. \\ \left. - \left[\frac{\partial}{\partial u_n} A_n^{\text{ir}}(u, u^*) + \frac{\partial}{\partial u_n^*} A_n^{\text{ir}*}(u, u^*) - \frac{\partial}{\partial u_n} A_n^{\text{rev}}(u, u^*) - \frac{\partial}{\partial u_n^*} A_n^{\text{rev}*}(u, u^*)\right] dt\right), \quad (\text{S8})$$

where $A_n^{\text{ir}}(u, u^*)$ and $A_n^{\text{rev}}(u, u^*)$ denote the irreversible and reversible parts of $A_n(u, u^*)$, respectively:

$$A_n^{\text{ir}}(u, u^*) := \frac{1}{2} [A_n(u, u^*) - A_n(-u, -u^*)] \\ = -\nu k_n^2 u_n, \quad (\text{S9})$$

$$A_n^{\text{rev}}(u, u^*) := \frac{1}{2} [A_n(u, u^*) + A_n(-u, -u^*)] \\ = B_n(u, u^*) + f_n. \quad (\text{S10})$$

By substituting (S7) and (S8) into (S6), we obtain

$$\Delta s^{\text{env}} = \sum_{n=0}^N \Delta s_n^{\text{env}}, \quad (\text{S11})$$

where

$$\Delta s_n^{\text{env}} := \frac{\rho}{2\nu k_n^2 k_B T} [A_n^{\text{ir}}(u, u^*) du_n^* - A_n^{\text{ir}}(u, u^*) A_n^{\text{rev}*}(u, u^*) dt] + \left[\frac{\partial}{\partial u_n} A_n^{\text{ir}}(u, u^*) - \frac{\partial}{\partial u_n} A_n^{\text{rev}}(u, u^*)\right] dt + \text{c.c.} \quad (\text{S12})$$

Note that, by using the Stratonovich product [4], this expression can be simply rewritten as

$$\Delta s_n^{\text{env}} = \frac{\rho}{2k_B T} \left\{ u_n^* \circ [(B_n(u, u^*) + f_n) dt - du_n] + u_n \circ [(B_n^*(u, u^*) + f_n^*) dt - du_n^*] \right\}. \quad (\text{S13})$$

The average medium entropy production can be calculated as

$$\langle \Delta s^{\text{env}} \rangle = \int du du^* p_t(u, u^*) \langle \Delta s^{\text{env}} | u, u^* \rangle, \quad (\text{S14})$$

where the conditional average $\langle \Delta s^{\text{env}} | u, u^* \rangle$ can be evaluated by replacing du_n (resp. du_n^*) with $A_n(u, u^*) dt$ (resp. $A_n^*(u, u^*) dt$) in Δs^{env} . Then, the medium entropy production rate reads

$$\frac{\langle \Delta s^{\text{env}} \rangle}{dt} = \sum_{n=0}^N \dot{S}_n^{\text{env}}, \quad (\text{S15})$$

where \dot{S}_n^{env} denotes the contribution from the n -th shell:

$$\dot{S}_n^{\text{env}} := \frac{\langle \Delta s_n^{\text{env}} \rangle}{dt} \\ = \int du du^* p_t(u, u^*) \left\{ \frac{\rho}{\nu k_n^2 k_B T} |A_n^{\text{ir}}(u, u^*)|^2 + \left[\frac{\partial}{\partial u_n} A_n^{\text{ir}}(u, u^*) - \frac{\partial}{\partial u_n} A_n^{\text{rev}}(u, u^*) + \text{c.c.} \right] \right\} \quad (\text{S16})$$

By combining (S4) and (S15), the second law of thermodynamics can be expressed as

$$\begin{aligned} \frac{d}{dt} S[u, u^*] + \frac{\langle \Delta s^{\text{env}} \rangle}{dt} &= \sum_{n=0}^N \int dud u^* \frac{\rho}{\nu k_n^2 k_B T} \frac{|J_n^{\text{ir}}(u, u^*)|^2}{p_t(u, u^*)} \\ &\geq 0, \end{aligned} \quad (\text{S17})$$

where $J_n^{\text{ir}}(u, u^*)$ denotes the irreversible current given by

$$\begin{aligned} J_n^{\text{ir}}(u, u^*) &= \frac{1}{2} [J_n(u, u^*) - J_n(-u, -u^*)] \\ &= A_n^{\text{ir}}(u, u^*) p_t(u, u^*) - \frac{2\nu k_n^2 k_B T}{\rho} \frac{\partial}{\partial u_n^*} p_t(u, u^*). \end{aligned} \quad (\text{S18})$$

Furthermore, since the total system $\{u, u^*\}$ can be considered as a $N + 1$ multipartite systems, i.e., each shell variable (u_n, u_n^*) experiences independent noise, it follows that the second law holds for each shell variable individually [5]:

$$\begin{aligned} \dot{S}_n[u, u^*] + \dot{S}_n^{\text{env}} &= \int dud u^* \frac{\rho}{\nu k_n^2 k_B T} \frac{|J_n^{\text{ir}}(u, u^*)|^2}{p_t(u, u^*)} \\ &\geq 0. \end{aligned} \quad (\text{S19})$$

B. Derivation of the second law of information thermodynamics

We now derive the second law of information thermodynamics for the bipartite systems $\mathbf{U}_K^<$ and $\mathbf{U}_K^>$ [5, 6]. First, we rewrite $\dot{S}_n[u, u^*]$ for $n \leq n_K$ as

$$\begin{aligned} \dot{S}_n[u, u^*] &= - \int dud u^* \left[J_n(u, u^*) \frac{\partial}{\partial u_n} \ln p_t(\mathbf{U}_K^< | \mathbf{U}_K^>) + J_n^*(u, u^*) \frac{\partial}{\partial u_n^*} \ln p_t(\mathbf{U}_K^< | \mathbf{U}_K^>) \right] \\ &= \dot{S}_n[\mathbf{U}_K^< | \mathbf{U}_K^>], \end{aligned} \quad (\text{S20})$$

where we have used $p_t(u, u^*) = p_t(\mathbf{U}_K^<, \mathbf{U}_K^>)$ and $\partial p_t(\mathbf{U}_K^>)/\partial u_n = \partial p_t(\mathbf{U}_K^>)/\partial u_n^* = 0$ for $n \leq n_K$. Note that $\dot{S}_n[\mathbf{U}_K^< | \mathbf{U}_K^>]$ is related to the learning rate through the following relation:

$$\begin{aligned} l_K^< &:= \frac{I[\mathbf{U}_K^<(t+dt) : \mathbf{U}_K^>(t)] - I[\mathbf{U}_K^<(t) : \mathbf{U}_K^>(t)]}{dt} \\ &= \frac{1}{dt} \left(S[\mathbf{U}_K^<(t+dt)] - S[\mathbf{U}_K^<(t+dt) | \mathbf{U}_K^>(t)] - S[\mathbf{U}_K^<(t)] + S[\mathbf{U}_K^<(t) | \mathbf{U}_K^>(t)] \right) \\ &= \frac{d}{dt} S[\mathbf{U}_K^<] - \sum_{n=0}^{n_K} \dot{S}_n[\mathbf{U}_K^< | \mathbf{U}_K^>]. \end{aligned} \quad (\text{S21})$$

From (S19)-(S21), we obtain the second law of information thermodynamics for $\mathbf{U}_K^<$,

$$\frac{d}{dt} S[\mathbf{U}_K^<] + \dot{S}_{\text{env}}^< \geq l_K^<, \quad (\text{S22})$$

where

$$\dot{S}_{\text{env}}^< := \sum_{n=0}^{n_K} \dot{S}_n^{\text{env}}. \quad (\text{S23})$$

Similarly, we can derive the second law of information thermodynamics for $\mathbf{U}_K^>$:

$$\frac{d}{dt} S[\mathbf{U}_K^>] + \dot{S}_{\text{env}}^> \geq l_K^>, \quad (\text{S24})$$

where

$$\dot{S}_{\text{env}}^> := \sum_{n=n_K+1}^N \dot{S}_n^{\text{env}}. \quad (\text{S25})$$

S2. DETAILS OF THE NUMERICAL SIMULATION

In this section, we explain the details of the numerical simulation. After describing the setup, the details of the KSG estimator are explained. In particular, we provide a detailed explanation of the method used to estimate the variance and bias of the KSG estimator. We also present the result in the deterministic case ($T = 0$).

A. Setup

To evaluate the inertial range straightforwardly, we first nondimensionalize the equation (1) with the Kolmogorov dissipation scale η and the velocity scale $u_\eta := (\epsilon\nu)^{1/4}$ by setting

$$\hat{u}_n := u_n/u_\eta, \quad \hat{k}_n := \eta k_n, \quad \hat{t} := t/\tau_\eta, \quad \hat{\xi}_n := (u_\eta/\eta)^{-1/2}\xi_n, \quad \hat{f}_n := f_n/F, \quad (\text{S26})$$

where $\tau_\eta := \eta/u_\eta$ denotes the typical time scale at the Kolmogorov dissipation scale, and F denotes the typical magnitude of the force per mass. The nondimensionalized equation (1) reads

$$\dot{\hat{u}}_n = \hat{B}_n(\hat{u}, \hat{u}^*) - \hat{k}_n^2 \hat{u}_n + (2\theta_\eta)^{1/2} \hat{k}_n \hat{\xi}_n + \mathcal{F}_\eta \hat{f}_n, \quad (\text{S27})$$

where

$$\hat{B}_n(\hat{u}, \hat{u}^*) := i \left(\hat{k}_{n+1} \hat{u}_{n+2} \hat{u}_{n+1}^* - \frac{1}{2} \hat{k}_n \hat{u}_{n+1} \hat{u}_{n-1}^* + \frac{1}{2} \hat{k}_{n-1} \hat{u}_{n-1} \hat{u}_{n-2} \right). \quad (\text{S28})$$

Here, $\theta_\eta := k_B T / \rho u_\eta^2$ denotes the ratio of the thermal energy to the kinetic energy at the Kolmogorov dissipation scale, and $\mathcal{F}_\eta := F\eta/u_\eta^2$ denotes the nondimensionalized magnitude of the force. Correspondingly, we set the shell index to be $n = M, \dots, R$ with $M = -[(3/4)\log_2(\text{Re})]$ and $R = N - M$, so that $k_0 = 1$ corresponds to the Kolmogorov dissipation scale.

We use a slaved 3/2-strong-order Ito-Taylor scheme [7] with the time-step $\delta\hat{t} := 10^{-5}$, which is smaller than the viscous time scale at the highest wavenumber $\hat{\tau}_{\text{vis}} := 1/\hat{k}_R^2 \sim 10^{-4}$. The parameter values are set to the same values used in [8, 9], which are consistent with the typical values in the atmospheric boundary layer (ABL). Specifically, the range of shell numbers is chosen as $n = -15, \dots, 7$ so that the achieved Reynolds number is comparable to the typical value in the ABL of $\text{Re} \sim 10^6$. To investigate the Re dependence of the LR, we also perform the numerical simulation for $\text{Re} \sim 10^5$ by setting $n = -12, \dots, 7$. In both cases, the dimensionless temperature is chosen as $\theta_\eta := 2.328 \times 10^{-8}$, and the external force acts only on the first two shells, i.e., $n_f = -14$ for $\text{Re} \sim 10^6$ and -11 for $\text{Re} \sim 10^5$. The values of the external forces are adjusted such that $\hat{u}_{\text{rms}} := \sqrt{\sum_{n=M}^R \langle |\hat{u}_n|^2 \rangle} \sim 10^2$ and $\hat{\epsilon} := \sum_{n=M}^R \hat{k}_n^2 \langle |\hat{u}_n|^2 \rangle \simeq 1$ [8, 9]: for $\text{Re} \sim 10^6$,

$$\begin{aligned} \mathcal{F}_\eta \hat{f}_{-15} &= -0.008900918232183095 - 0.0305497603210104i, \\ \mathcal{F}_\eta \hat{f}_{-14} &= 0.005116337459331228 - 0.018175040700335127i, \end{aligned} \quad (\text{S29})$$

while for $\text{Re} \sim 10^5$,

$$\begin{aligned} \mathcal{F}_\eta \hat{f}_{-12} &= -0.017415685046854878 - 0.05977417049893835i, \\ \mathcal{F}_\eta \hat{f}_{-11} &= 0.010010711194151034 - 0.03556158772544649i. \end{aligned} \quad (\text{S30})$$

In the averaging of the energy spectrum and the estimation of the MI, we use $N_{\text{samp}} = 3 \times 10^5$ samples. For the case of $\text{Re} \sim 10^6$, these samples are obtained by sampling 100 snapshots at time $\hat{t} = 1000i$ ($i = 1, 2, \dots, 100$) for each of the 3000 noise realizations. That is, for each of the 3000 independent runs, we sample 100 snapshots. Here, the time interval of the sampling, 1000, is chosen to be larger than one large-eddy turnover time $\tau_L/\tau_\eta \simeq 734 < 1000$. Similarly, for the case of $\text{Re} \sim 10^5$, $N_{\text{samp}} = 3 \times 10^5$ samples are obtained by sampling 100 snapshots at time $\hat{t} = 500i$ ($i = 1, 2, \dots, 100$) for each of the 3000 noise realizations, where the time interval, 500, is chosen to be larger than one large-eddy turnover time $\tau_L/\tau_\eta \simeq 181 < 500$.

B. The KSG estimator

The KSG estimator for the mutual information $I[X : Y]$ (either or both of the random variables X and Y can be multidimensional) is defined as follows [10]:

$$\hat{I}_{\text{KSG}}^{(k)}[X : Y] := \psi(k) - 1/k + \psi(N_{\text{samp}}) - \frac{1}{N_{\text{samp}}} \sum_{i=1}^{N_{\text{samp}}} [\psi(n_x(i)) + \psi(n_y(i))], \quad (\text{S31})$$

where $k \in \mathbb{N}$ denotes the parameter of the KSG estimator, ψ is the digamma function, N_{samp} denotes the total number of samples, and $n_\alpha^{(k)}(i)$ ($\alpha = x, y$) is the number of samples such that $\|\alpha_j - \alpha_i\| \leq \epsilon_\alpha^{(k)}(i)/2$. Here, $\epsilon_\alpha^{(k)}(i)$ denotes the α extent of the smallest hyper-rectangle in the (x, y) space centered at the i -th sample (x_i, y_i) that contains k of its neighboring samples. While any norms can be used for $\|\alpha_j - \alpha_i\|$, we use the standard Euclidean norm here.

Note that k is the only free parameter of the KSG estimator. By varying k , we can detect the structure of the underlying probability distribution in different spatial resolutions. To choose the optimal k (if it exists), we must estimate both the standard deviation and the bias of the KSG estimator [11].

C. Estimation of the variance of the KSG estimator

In this section, we explain the method used to estimate of the variance of the KSG estimator based on the subsampling approach proposed by Holmes and Nemenman [11]. This method is based on the fact that the variance of any function that is an average of N i.i.d. random variables scales as $1/N$. Therefore, we write the variance of the KSG estimator as

$$\text{Var}_{N_{\text{samp}}}[\hat{I}_{\text{KSG}}^{(k)}] = \frac{B^{(k)}}{N_{\text{samp}}}. \quad (\text{S32})$$

We estimate $B^{(k)}$ via a subsampling approach. Specifically, we first partition the $N_{\text{samp}} = N$ samples into n nonoverlapping subsets of equal size as much as possible. Let $\hat{I}_{\text{KSG},i}^{(k)}(N/n)$ be the i -th realization of $\hat{I}_{\text{KSG}}^{(k)}[X : Y]$ with $N_{\text{samp}} = N/n$ ($i = 1, 2, \dots, n$). Then, we calculate the unbiased sample variance of these n values of $\hat{I}_{\text{KSG},i}^{(k)}(N/n)$:

$$\sigma_{k,N/n}^2 := \frac{1}{n-1} \sum_{i=1}^n \left(\hat{I}_{\text{KSG},i}^{(k)}(N/n) - \frac{1}{n} \sum_{i=1}^n \hat{I}_{\text{KSG},i}^{(k)}(N/n) \right)^2. \quad (\text{S33})$$

This is our estimate of $\text{Var}_{N/n}[\hat{I}_{\text{KSG}}^{(k)}] = nB^{(k)}/N$. Finally, we estimate $B^{(k)}$ by using maximum likelihood estimation. In doing so, we first calculate $\sigma_{k,N/n_\ell}^2$ for various n_ℓ ($\ell = 1, 2, \dots, L$). Then, from Cochran's theorem, $(n_\ell - 1)\sigma_{k,N/n_\ell}^2/\text{Var}_{N/n_\ell}[\hat{I}_{\text{KSG}}^{(k)}]$ follows the χ^2 -distribution with $n_\ell - 1$ degrees of freedom:

$$P_{n_\ell-1}^{(\chi^2)}(x) := \frac{1}{2^{(n_\ell-1)/2}\Gamma(\frac{n_\ell-1}{2})} x^{\frac{n_\ell-1}{2}-1} e^{-x/2}. \quad (\text{S34})$$

By assuming independence of $\{\sigma_{k,N/n_\ell}^2\}_{\ell=1}^L$, a likelihood function for $B^{(k)}$ is

$$\prod_{\ell=1}^L P_{n_\ell-1}^{(\chi^2)} \left(\frac{N(n_\ell - 1)\sigma_{k,N/n_\ell}^2}{B^{(k)}n_\ell} \right). \quad (\text{S35})$$

We then obtain the maximum likelihood estimator:

$$\begin{aligned} \hat{B}^{(k)} &:= \arg \max_{B^{(k)}} \prod_{\ell=1}^L P_{n_\ell-1}^{(\chi^2)} \left(\frac{N(n_\ell - 1)\sigma_{k,N/n_\ell}^2}{B^{(k)}n_\ell} \right) \\ &= \frac{\sum_{\ell=1}^L \frac{n_\ell-1}{n_\ell} N \sigma_{k,N/n_\ell}^2}{\sum_{\ell=1}^L (n_\ell - 3)}. \end{aligned} \quad (\text{S36})$$

By combining (S32) and (S36), we can estimate the variance of the KSG estimator to be $\hat{B}^{(k)}/N_{\text{samp}}$.

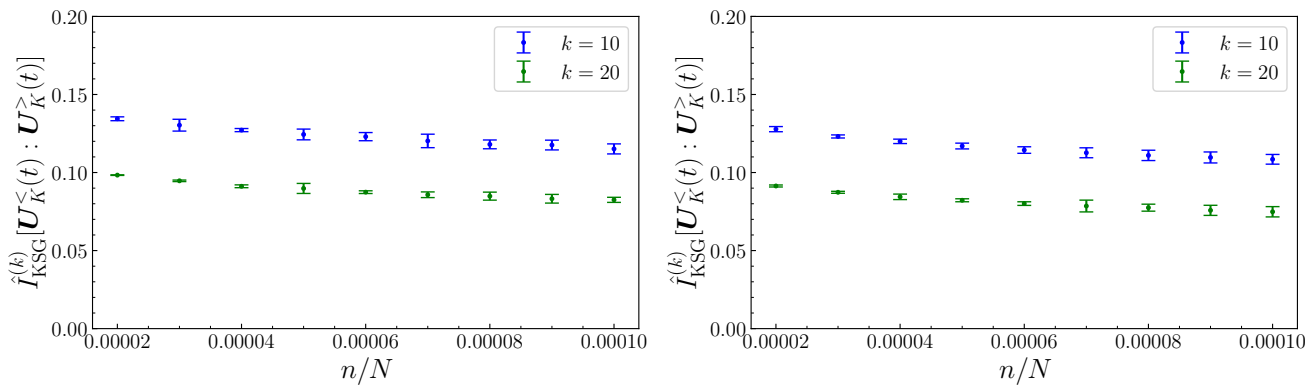


FIG. S1. (color online). Bias of the KSG estimator $\hat{I}_{\text{KSG}}^{(k)}[\mathbf{U}_K^<(t) : \mathbf{U}_K^>(t)]$ as a function of $1/N_{\text{samp}} = n/N$ with $n = 2, 3, \dots, 10$ and $N = 10^5$. $K = k_{10}$ (left) and $K = k_{15}$ (right).

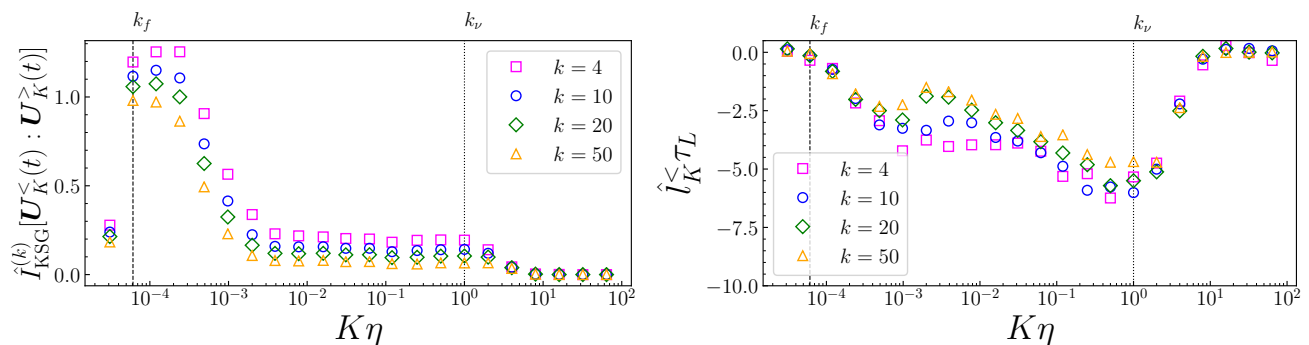


FIG. S2. (color online). Scale dependences of the estimated MI $\hat{I}_{\text{KSG}}^{(k)}[\mathbf{U}_K^<(t) : \mathbf{U}_K^>(t)]$ (left) and LR $\hat{I}_K^<$ (right). Note that the LR is plotted in units of the inverse of τ_L .

D. Estimation bias of the KSG estimator

Although the KSG estimator is asymptotically unbiased for sufficiently regular probability distributions as $N_{\text{samp}} \rightarrow \infty$, both sample-size-dependent bias and k -dependent bias generally exist for a finite N_{samp} [11]. The sample-size-dependent (resp. k -dependent) bias can be detected by comparing the sample-size-dependence (resp. k -dependence) of the estimated MI with its standard deviation. If the sample-size-dependence (resp. k -dependence) of the estimated MI is much larger than its standard deviation, then a sample-size-dependent (resp. k -dependent) bias may be present.

Note that k is related to the spatial resolution in detecting the structure of the underlying probability distribution. For large k , because the fine structure of the probability distribution cannot be detected, we would expect the MI to be underestimated. At the same time, because $n_x(i)$ and $n_y(i)$ both increase with increasing k , the standard deviation of the estimated MI will be smaller for large k . If there is no k -dependent bias, we can choose the optimal k such that there is no sample-size-dependence compared to the standard deviation and the standard deviation is the smallest.

Figure S1 shows bias of the KSG estimator $\hat{I}_{\text{KSG}}^{(k)}[\mathbf{U}_K^<(t) : \mathbf{U}_K^>(t)]$ as a function of $1/N_{\text{samp}} = n/N$ with $N = 10^5$ in the case of $\text{Re} \sim 10^6$. Here, we use $n = 2, 3, \dots, 10$, following [11]. The wave number K is within the inertial range, $K = k_{10}$ (left), and at the Kolmogorov dissipation scale, $K = k_{15}$ (right). The error bars are estimated by using the unbiased sample variance (S33). From (S32) and (S36), the standard deviation of $\hat{I}_{\text{KSG}}^{(k)}[\mathbf{U}_K^<(t) : \mathbf{U}_K^>(t)]$ is estimated to be $\sim 10^{-3}$ for $N_{\text{samp}} \sim 10^5$. It can be seen from Fig. S1 that, while there is no significant sample-size-dependent bias, a k -dependent bias does exist. In particular, the estimated MI is underestimated as k is increased.

Figure S2 shows the scale dependences of the estimated MI and LR for $k = 4, 10, 20, 50$ with $N_{\text{samp}} = 2 \times 10^5$ in the case of $\text{Re} \sim 10^6$. Here, $k = 4$ is chosen because $k = 2, 3, 4$ are recommended in [10]. This results clearly show that the estimated MI and LR are underestimated as k is increased. Therefore, it is difficult to choose the optimal k in this case. The important point here is that the estimated LR is negative for K within the inertial range for all k . As mentioned in the main text, we remark that the error bar of the LR $\hat{I}_K^<$ is of the same order as $\hat{I}_K^<$ itself if we naively estimate it by using the estimated standard deviation of the MI.

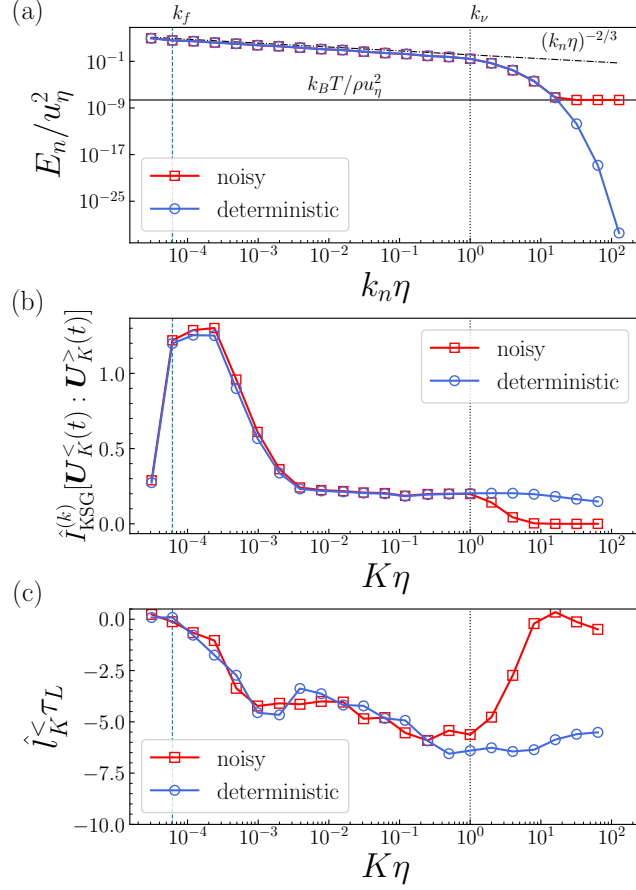


FIG. S3. (color online). (a) Scale dependence of the energy spectrum $E_n = \langle |u_n|^2 \rangle_{ss}/2$. The dash-dotted line represents $\epsilon^{2/3} k_n^{-2/3}$. The solid line represents the thermal equipartition value $k_B T / \rho$. (b) Scale dependence of the estimated MI $\hat{I}_{KSG}^{(k)}[U_K^<(t) : U_K^>(t)]$ with $k = 4$. The error bars are within the marker size. (c) Scale dependence of the estimated LR $\hat{I}_K^{<}$. Note that it is plotted in units of the inverse of the τ_L . In all panels, the dotted and dashed lines represent the Kolmogorov dissipation scale $k_\nu = 1/\eta$ and injection scale k_f , respectively. The noisy case is the same as the one presented in the main text (cyan line in Fig. 2).

E. Deterministic case

Here, we present the result in the deterministic case ($T = 0$). We calculate the deterministic case by setting $\theta_\eta = 0$ in the Ito-Taylor scheme (Sec. S2 A). Other parameters are the same as in the noisy case with $N = 22$. As independent initial-data, we use the snapshots in the noisy case at time $\hat{t} = 10^5$. We have used $N_{\text{samp}} = 2 \times 10^5$ samples in the following averaging and estimation. These samples are obtained by sampling 100 snapshots at time $\hat{t} = 1000i$ ($i = 1, 2, \dots, 100$) for each of the 2000 independent runs.

Figure S3(a) shows the energy spectrum $E_n := \langle |u_n|^2 \rangle_{ss}/2$ in the steady state. The achieved Reynolds number in the deterministic case is $\text{Re} \simeq 1.46 \times 10^6$. In the inertial range, both the deterministic and noisy cases exhibit the Kolmogorov spectrum. In the dissipation range, in contrast, the deterministic case shows a rapid exponential decay.

Figure S3(b) shows the estimated MI $\hat{I}_{KSG}^{(k)}[U_K^<(t) : U_K^>(t)]$ with $k = 4$. Its standard deviation is also estimated to be $\sim 10^{-3}$ by subsampling, which lies within the marker size. While the deterministic case is almost the same as the noisy case in the inertial range, it takes a finite value even in the dissipation range. In other words, the correlation between large and small scales is not destroyed because of the absence of thermal fluctuations.

In Fig. S3(c), we show the estimated LR $\hat{I}_K^{<}$ in units of the inverse of the large-eddy turnover time τ_L . In the deterministic case, we find that $\tau_L \simeq 732\tau_\eta$. From this figure, we can see that the LR in the deterministic case takes almost the same value as in the noisy case in the inertial range. This result implies that the information flow itself is mainly governed by the large-scale dynamics rather than by the thermal fluctuations. In contrast, it takes finite negative value in the dissipation range. In other words, in the absence of thermal fluctuations, the information flow

reaches the far dissipation range.

- [1] H. Risken, *The Fokker-Planck Equation* (Springer, 1996).
- [2] R. E. Spinney and I. J. Ford, Entropy production in full phase space for continuous stochastic dynamics, *Phys. Rev. E* **85**, 051113 (2012).
- [3] C. Maes, Local detailed balance, *SciPost Phys. Lect. Notes* **32**, 1 (2021).
- [4] C. W. Gardiner, *Handbook of Stochastic Methods*, 4th ed. (Springer, Berlin, 2009).
- [5] J. M. Horowitz, Multipartite information flow for multiple Maxwell demons, *J. Stat. Mech.* , P03006 (2015).
- [6] J. M. Horowitz and M. Esposito, Thermodynamics with continuous information flow, *Phys. Rev. X* **4**, 031015 (2014).
- [7] G. J. Lord and J. Rougemont, A numerical scheme for stochastic PDEs with Gevrey regularity, *IMA J. Numer. Anal.* **24**, 587 (2004).
- [8] D. Bandak, N. Goldenfeld, A. A. Mailybaev, and G. Eyink, Dissipation-range fluid turbulence and thermal noise, *Phys. Rev. E* **105**, 065113 (2022).
- [9] D. Bandak, G. L. Eyink, A. Mailybaev, and N. Goldenfeld, Thermal noise competes with turbulent fluctuations below millimeter scales, arXiv preprint arXiv:2107.03184 (2021).
- [10] A. Kraskov, H. Stögbauer, and P. Grassberger, Estimating mutual information, *Phys. Rev. E* **69**, 066138 (2004).
- [11] C. M. Holmes and I. Nemenman, Estimation of mutual information for real-valued data with error bars and controlled bias, *Phys. Rev. E* **100**, 022404 (2019).